PII: S0955-2219(98)00117-4
Printed in Great Britain. All rights reserved
0955-2219/98/$—see front matter

Enstatite Based Ceramics for Machinable Prosthesis Applications

D. Goeuriot,[a]* J. C. Dubois,[b] D. Merle,[a]† F. Thevenot[a] and P. Exbrayat[b]

[a]Ecole Nationale Superieure Des Mines De Saint-Etienne, 158 cours Fauriel, F-42023 Saint-Etienne Cédex 2, France
[b]Faculte D'Odontologie De Lyon, Domaine de la Buire, Rue Guillaume Paradin, F-69008 Lyon, France

(Received 24 December 1997; revised version received 22 March 1998; accepted 9 April 1998)

Abstract

Fabrication and properties of polycrystalline ceramics from talcs are described. Two types of talcs, lamellar and equiaxe, were dehydrated, attrition milled (0·5 to 4 h), pressed and sintered. Dilatometric studies and XRD analyses were used to determine phase transformations into enstatite during heat treatment. The soaking temperature leading to the highest densities must be chosen to avoid clinoenstatite formation, that gives porosity. A CaO–P_2O_5–$AlPO_4$–Al_2O_3 glass addition (up to 15 wt%) lowers the sintering temperature of 50°C. Flexural strength and toughness are higher than those of dental commercial glass ceramics, and cutting grooves do not chip. Biocompatibility is also studied: those enstatite ceramics enhance the deposit of mineralized bone tissue. These enstatite ceramics could be good candidates for dental (implants or crowns) or bone restorations. *© 1998 Elsevier Science Limited. All rights reserved*

1 Introduction

Several research groups are actively engaged in applying CAD-CAM systems (Computer Aided Design-Computer Aided Manufacturing) for producing dental prostheses.[1] CAD-CAM can also be applied to the fabrication of bone restorations.

For example, a French system[2] uses a laser camera to produce images of the patient's mouth. Data are processed by shape recognition software, visualised on a video display, and transfered to a CAD-CAM software package that creates a three dimensional model of the environment where the prosthesis will be ultimately fitted. The interactive capability of the CAD-CAM software allows the dentist to have access to a library describing 'theoretical teeth', to adapt them to the patient's oral environment, and to design a three dimensional model of the prosthesis on the computer screen. The CAD-CAM software computes the instrument paths needed and micro milling machine cuts the tooth.

The present paper deals with fabrication and properties of a new polycrystalline material for these biomedical applications: enstatite ($MgSiO_3$), which has suitable advantages: colour from white to brown for dental crowns, sheet structure favourable to machinability. Enstatite based materials are compared with available dental ceramics (alumina and glass ceramics): mechanical properties and machining tests (Fig. 1). Biocompatibility tests are also described.

*To whom correspondence should be addressed. Fax: +33 77 420 000; e-mail: dgoeurio@emse.fr
Present address: Vesuvius France, 68 Rue Paul Deudon, B.P. 19, F-59750 Feignies, France.

2 Experimental methods

2.1 Fabrication of enstatite-based materials

2.1.1 Enstatites

Talc has a mica like structure with piled sheets.

Two types of 'talc de Luzenac': 15M00 and SS-C were dehydrated at 1200°C for 3 h. The powder then obtained was a mixture of enstatite and cristobalite:

$$3MgO{\cdot}4SiO_2{\cdot}H_2O \rightarrow 3MgO{\cdot}SiO_2 + SiO_2 + H_2O \nearrow$$

The two powders, 15M00, elongated (lamellar) grains, and SS-C, equiaxed grains, were attrition milled (from 0·5 to 4 h) in order to obtain six batches with a grain size from 4·7 to 1 mm (Fig. 1). The elongated grains (15M00) became pseudo-spherical when the attrition milling time increased. Initial talc contained mineral impurities

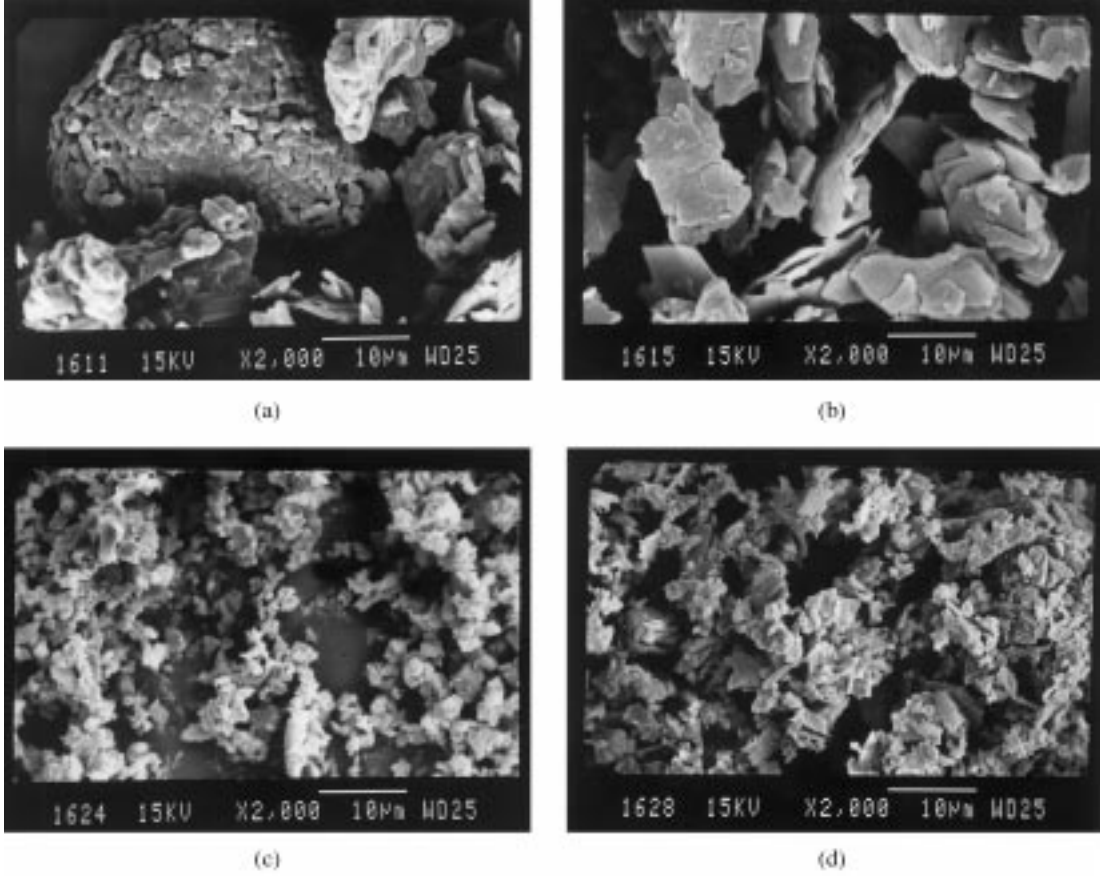

Fig. 1. Initial and treated talc (talc de LUZENAC FRANCE) powders. (a) SS-C dehydrated, equiaxed grains; (b) 15M00 dehydrated, elongated grains; (c) SSC1: SS-C dehydrated and attrition milled (1 h); (d) 15M1: 15M00 dehydrated and attrition milled (1 h).

as chlorite, dolomia that lead to few percent of oxides: Al_2O_3,Fe_2O_3,CaO (Table 1). Powders were then pressed (uniaxial and isostatic pressures, respectively 30 and 200 MPa) with bonding agents, fired and sintered (heating rate: 2°C min^{-1}, soaking time: 2 h, cooling rate: 5°C min^{-1}. Samples references are explained in Table 2.

2.1.2 Biosteatites

So called biosteatites are enstatite materials sintered with added glass in order to lower their sintering temperature.

The glass composition was chosen in the CaO–P_2O_5–$A1PO_4$–$A1_2O_3$ system because of its biocompatibility and low melting point. Three glasses were obtained by a mixture of dehydrated $(PO_4)\cdot 2H_2O$, $A1PO_4\cdot 4H_2O$ and $A1_2O_3$ (0·25 μm): a basic glass composed of 80 wt% $CaO\cdot P_2O_5$ –20% $A1PO_4$ (CPA), the same with 2·5 wt% (CPA2) and 5 wt% $A1_2O_3$ (CPA5). Mixtures were melted at 1200°C for 2 h in a aluminosilicate crucible and quenched in cold water. Then the glass powder was milled to obtain an average grain size of 1·5 μm. The glassy phase was incorporated in enstatite by magnetic mixer in alcohol medium with dispersant and binder, dried and sieved at 200 μm.

Sintering studies were performed using enstatite with elongated grains milled during 1 h, that leads to the best mechanical properties (15 M1), with addition of 5, 10, 15% CPA, CPA2 and CPA5. Samples are named 15 M X Y:

X: 0, 2 or 5 means the use of CPA, CPA2, CPA5;

Y: 0, 5, 10 is the amount of glass in the mixture (wt%).

Table 1. Initial talcs composition (wt%)

Oxide (wt%)	*SS-C*	*15M00*
SiO_2	61·8	60
MgO	31	32
Al_2O_3	0·2	2
Fe_2O_3	0·3	0·8
CaO	0·6	0·9
Firing weight loss (1050°C)	5·6	5·2
Mineral (wt%)		
Talc	98	92
Chlorite	trace	6
Doloma	1·5	1

2.2 Characterization of materials

Scanning electron microscopy (SEM) observations were performed on fracture faces or polished surfaces. *Fracture strength* was obtained by three point bending test with a crosshead speed of 0·1 mm min^{-1} on a universal testing machine

(INSTRON). *Young's modulus* was determined by ultrasonic method. Concerning fracture toughness, the cracks were made by KVAM's precracking method.[3] On each specimen a KNOOP diamond was used to make overlapping indentations in a straight line across one of the narrow sides. A load of 49 N (5 kgf) was used to make the hardness indentation on commercial dental ceramics and a load of 153 N (15 kgf) for enstatite-based material. The cracks were made visible by immersing the specimens in a dye penetrant liquid. Then each specimen was bent to fracture in a three point bending test with a crosshead speed of $0{\cdot}1\ \mathrm{mm\ min^{-1}}$.

The *weight-load-cutting testing machine* that permits comparison of the material machinability is described in Fig. 2. The diamond tool (grain size 76 mm) was driven by an air-turbine grinding machine while the ceramic specimen was fixed on a table that was moved by an applied load. Samples were polished before machining. The time taken by the bur to go from side to side of the specimen permitted calculation of the average cutting speed for different materials. The tool was lubricated by water based lubricant during machining. The cutting parameters were: load (F), bur rotating speed (ω, measured by a stroboscope), cutting depth (e). Machined grooves were observed by optical and scanning electron microscopy.

The *biological evaluation* of biosteatites is based on the ultrastructural study of rat bone cells grown on samples of 15M1 ceramics, on the one hand, and, on the other hand on the measurement of alkaline phosphate activity (ALP activity). The protocols used were respectively those defined by Exbrayat[4] and by Veron.[5]

3 Results and discussion

3.1 Enstatite-based materials

During the different heating treatments (dehydration, sintering) some crystallographic changes occur that have consequences on the material microstructure. This problem is detailed in the next paragraph.

3.1.1 Crystallographic changes during the enstatite fabrication

The different enstatite polymorphs and changes from one form to another are described on Fig. 3.[6,7] The stable form at high temperature is proto-enstatite and at low temperature orthoenstatite. A metastable form clinoenstatite can be formed from ortho- or protoenstatite depending on temperature, pressure, dopants, internal stresses in grains, grain size.[8,9]

3.1.1.1. Dehydration and attrition milling. XRD analyses [Fig. 4(a)] showed that 15M00 converts after dehydration into ortho and SS-C to protoenstatite. This difference could be due to the conditions of the mineral talc formation: low pressure for SS-C and high pressure for 15M00, that could induce stresses leading to the ortho enstatite form in 15M00. Also the impurities present in 15M00 are favourable to the proto→ortho transformation during cooling.

During attrition milling, grains are submitted to shear stresses. Clinoenstatite formation from proto is favoured by these stresses.[9] So, in the case of dehydrated SS-C talc, the clino phase appeared even for 0·5 h milling time, and is the major phase after 4 h [Fig. 4(b)]. A small amount of clinoenstatite was formed in 15M00 only after 4 h attrition [Fig. 4(b)].

3.1.1.2. Cooling after sintering. From XRD, it was verified that during the soaking time, materials from both enstatites were in the proto form. As shown in Fig. 5, some of the samples, mainly those sintered at high temperature (for example 15M1 sintered at 1450°C during 2 h) contained many

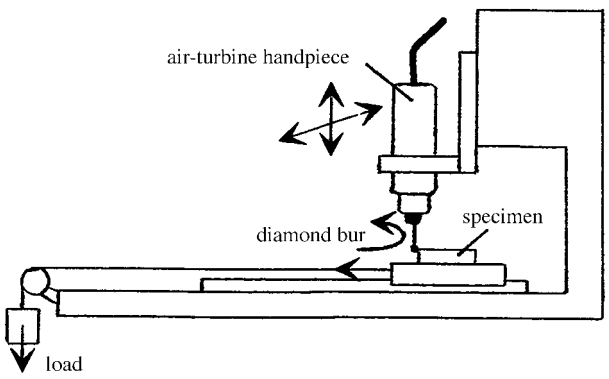

Fig. 2. Machinability test.

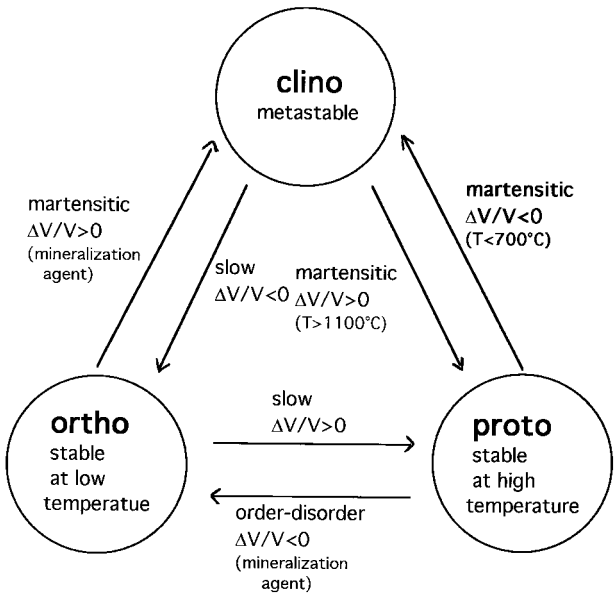

Fig. 3. Polymorphism of enstatite.

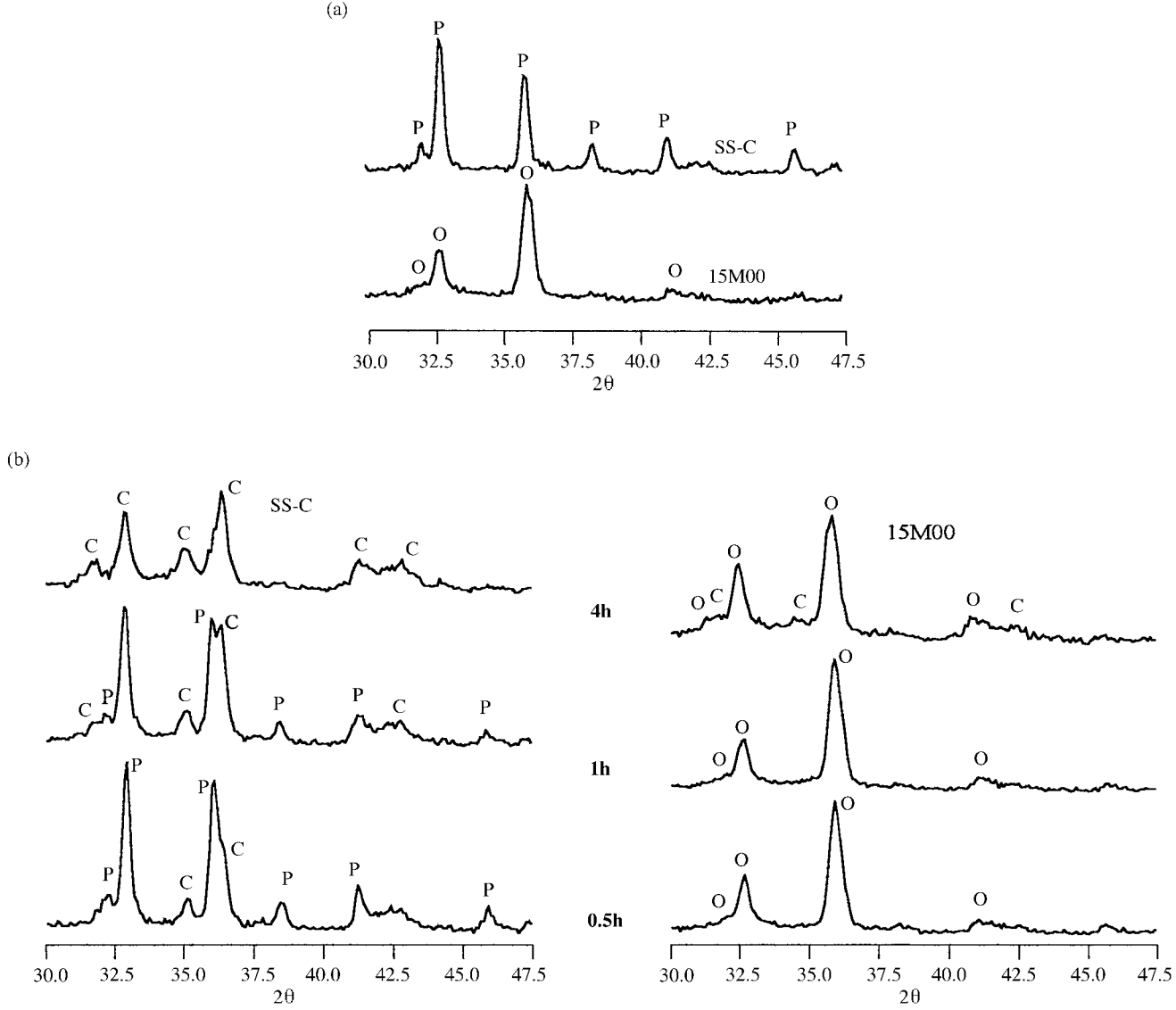

Fig. 4. Effect of dehydration and milling on enstatite transformations; (a) after dehydration; (b) after attrition milling (0·5, 1, 4 h); O: ortho, P: proto, C: clinoenstatite.

large pores. XRD suggested this porosity was related to the presence of the clinoenstatite form. The transformation occured during cooling and apparently, there is a higher tendency for large protoenstatite crystals to convert into clinoenstatite than for small ones. This transformation is thought to be a martensitic type and leads to a volume decrease from 3 to 6%.[6–10] This explains the large porosity in samples sintered at high temperatures, in which grain growth occurs ; the resulting microstructures will induce low mechanical properties.

3.1.1.3. Conclusion. To choose the sintering temperature, soaking temperatures around those corresponding to the highest sintering rate TM, determined by a dilatometric study were tested in a range TM ± 50°C.

XRD analyses permitted removal of samples containing clinoenstatite. Moreover, SEM observations of fracture faces permitted selection of the temperature (Table 2) when samples had lower and finer porosity and smaller grain size. The chosen sintering temperatures were similar for both enstatites and decrease with the initial powder grain size: 1375, 1350 and 1275°C for enstatites respectively milled during 0·5, 1 and 4 h.

3.1.2 Properties of enstatite materials

Specimens sintered at the precedent chosen temperatures had properties presented in Table 2 that can be related to their microstructure (Fig. 6). Material from the elongated grains (initial talc: 15M00) presented remaining anisotropic grains (15M0, 15Ml), the others were pseudospherical.

Globally, both enstatites had different behaviours: for the one with elongated grains (initial talc: 15M00) fracture toughnesses were the highest, and for the equiaxial one (initial talc: SS-C) the flexural strengths were the highest. This is due to the grain morphology:

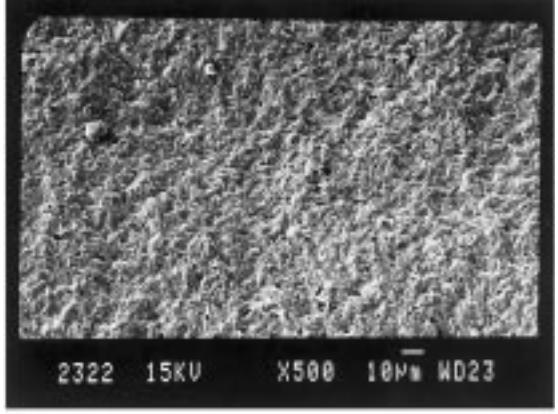

(a)

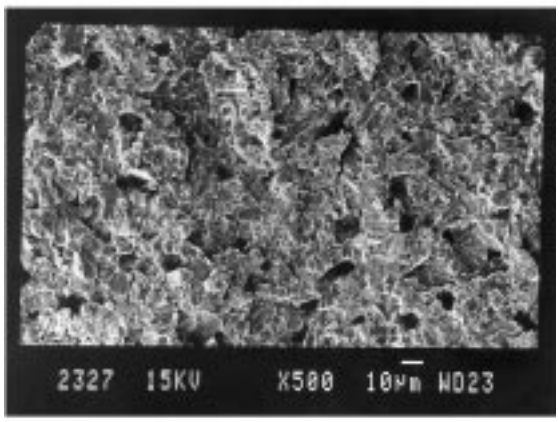

(b)

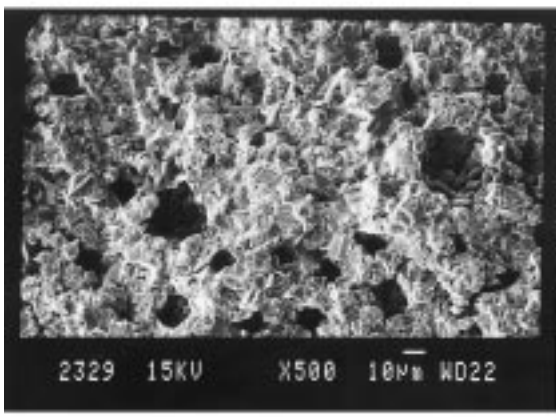

(c)

Fig. 5. Fracture surfaces of 15M1 enstatite sintered at: (a) 1350°C-2 h containing protoenstatite; (b) 1425°C-2 h containing proto + clinoenstatite; (c) 1450°C-2 h containing clinoenstatite.

- on one side, as for silicon nitride, for example,[11] elongated grains lead to crack deflection. The fracture propagates in this case rather along the crystal sheets than across,
- on the other side, this lamellar morphology, and also the porosity, that is larger in amount and size in 15M materials, is unfavourable to the flexural strengths.

Flexural strengths presented slight evolutions with the grain size.

For 15M0, 15M1 and 15M4 the slight decrease of thoughness with the grain size can be attributed to an aspect ratio decrease. The lower thoughness of SSC4 could be explained by a glassy phase at the grain boundaries created by impurities (initial and due to the long milling treatment).

Hardnesses increased when the grain size decreased in relation also with a porosity decrease.

The enstatite ceramics were compared with two commercial glass ceramics containing leucite: $K_2O{\cdot}Al_2O_3{\cdot}4SiO_2$ (IVOCLAR) or tetrafluoromica crystals $KMg_{2,5}\ Si_4O_{10}F_2$ (DICOR from CORNING-GLASS). Comparing to those commercial glass ceramics, the enstatites presented similar flexural strength as DICOR and much higher than IVOCLAR. Enstatites toughnesses were much higher than those of commercial dental ceramics.

3.2 BioSteatite

As mentioned before, so-called 'biosteatites' are enstatite materials sintered with added glass in order to lower their sintering temperature. The glassy phase could improve also their aspect bringing them some translucency.

3.2.1 Sintering

Dilatometric curves (Fig. 7) were similar for the three glasses (only 15M2Y is shown). The shrinkage began at lower temperature for samples containing glass, the lowest for the highest glass amount.

The shrinkage rate increased in the range 1010–1130°C then was slowed down between 1130–1160°C and then increased again. Final samples sintered at temperatures chosen by the same way as for single enstatite (Table 3) contained pores that are very large (up to 50 μm) for steatite containing 15% glass without alumina [Fig. 8(a)]. Samples containing 5% glass had only few small pores, less than in 15M1 [Fig. 8(d)–(f)].

Dilatometric curves can be explained by physico-chemical evolutions in the materials (Fig. 7):

- First increase of shrinkage rate.
  It is due to a liquid formation. D.T.A. analyses showed that for glasses the melting point is about 1200°C, but for 15 MXY a reaction took place at about 1100°C, whatever the glass composition. It can be supposed that this reaction gives a liquid phase that explains the high shrinkage rate observed on dilatometric curves.

  Independently, several other mixtures: $15M1 + AlPO_4$, $15M1 + Al_2O_3$ and $15M1 + CaO{\cdot}P_2O_5$ which composition corresponds to those of 15M1 mixture were

Table 2. Sintering conditions and properties of enstatites dehydrated (1 h) and milled [15MX, X time = 0(0·5 h), 1(1 h), 4 (4 h)]

Sample reference	d_{50} (μm)	*Attrition time (h)*	*Sintering temperature (°C)*	*Density (g/cm³)*	σ_f *± 20 MPa*	*KIC ± 0·1 MPa·√m*	*HV (± 50) (Vickers)*	E *(GPa)*
15M0*	4·6	0·5	1375	2·88	185	2·4	490	180
15M1*	2·7	1	1350	2·88	200	2·2	520	180
15M4*	1	4	1275	2·88	190	2	590	185
SSC0*†	4·7	0·5	1375	2·83	220	1·7	500	130
SSC1†*	2·7	1	1350	2·86	250	1·6	580	130
SSC4*†	1	4	1250	2·87	210	1·2	680	140
DICOR				2·77	240	0·8	360	80
IVOCLAR				0·44	115	0·7	530	60

* Enstatite from talcs with elongated grains.
† Enstatite from talcs with equiaxed grains.
σ_f: flexural strength; KIC: fracture toughness; HV: hardness; E: Young's modulus. DICOR: glass ceramic containing tetrafluoromica crystals: $KMg_{2.5}Si_4O_{10}F_2$. IVOCLAR: glass ceramic containing leucite: $K_2O{\cdot}Al_2O_3{\cdot}4SiO_2$.

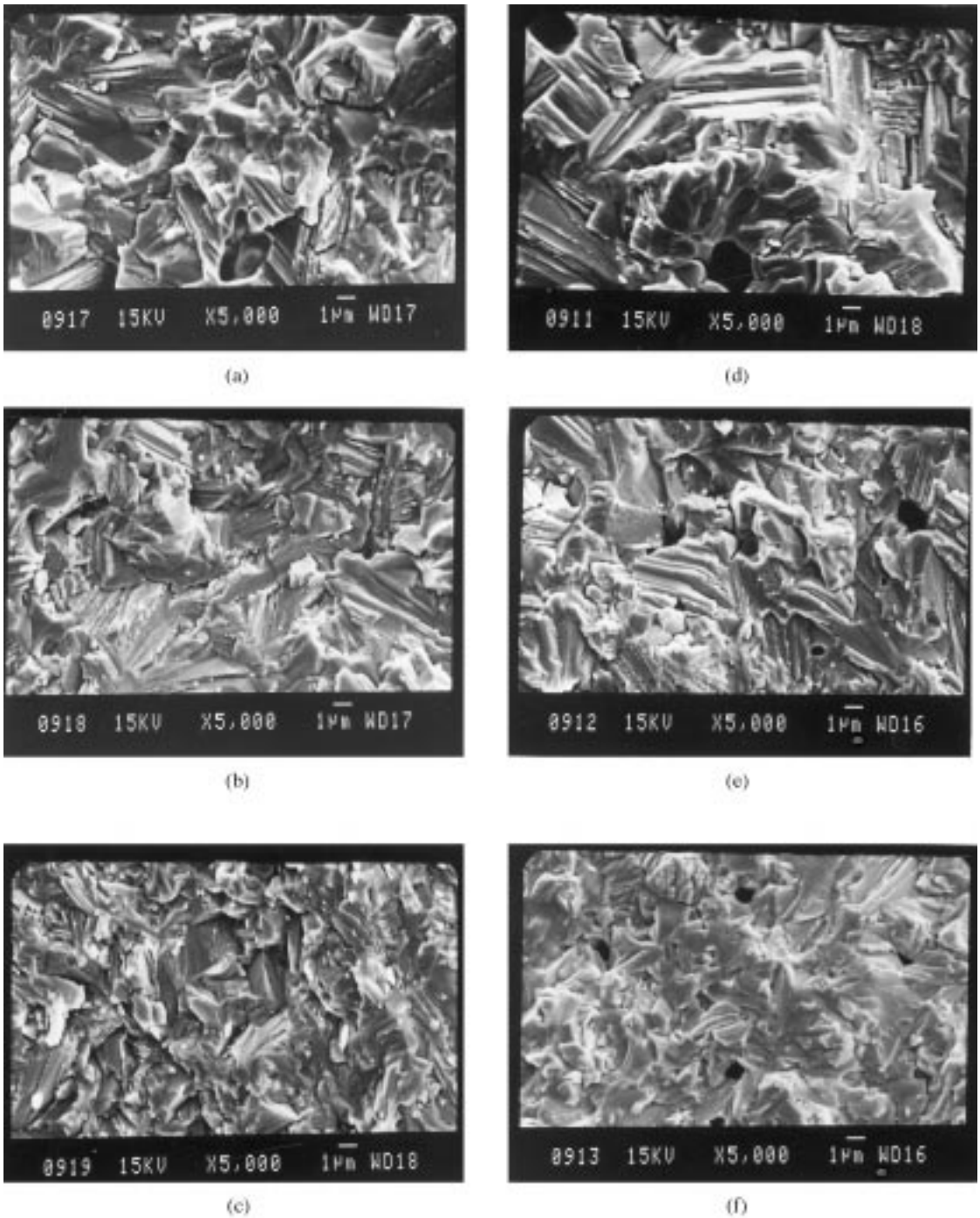

Fig. 6. Fracture surfaces of the different enstatites (cf. Table 2): (a) SSC0; (b) SSC1; (c) SSC4; (d) 15M0; (e) 15M1; (f) 15M4.

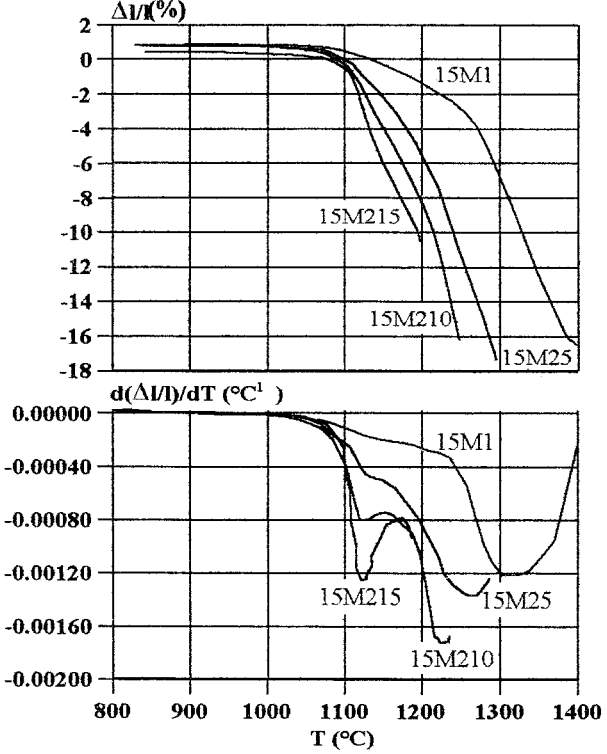

Fig. 7. Dilatometric curves for 15MXY mixtures: example of 15M1 + 5, 10 and 15% CPA2 (80 wt% $CaO{\cdot}P_2O_5$ + 20 wt% AlPO4 + 2.5 wt% Al_2O_3), named 15M25, 15M210 and 15M215.

made, and analysed by D.T.A. That showed that the reaction took place mainly between enstatite or silica of 15M1, and calcium phosphate (CP).

- Shrinkage slowing down.
  As for enstatite material (15M1), it is due to the ortho → protoenstatite transformation (controlled by XRD analyses) but it takes a shorter range of temperature: 1125–1175°C than for 15M1 (1125–1275°C). So the glass is favourable to this transformation.
- Final remaining porosity.
  This porosity was important especially for material with a high glass content. An explanation can be given considering previous studies:
  - Glass sintering condition.
    F. Pernot[12] used a glass which had a similar composition to make porous glass–ceramic by crystallizing-sintering of glass powder for prosthetic applications. But to have pores, $CaCO_3$ foaming agent was added to the glass. The crystallisation process of porous material was explained as follows: initially before carbonate starts reacting, the sintering of glass particles enclose CaCO3 particles: glass $CaO{\cdot}P_2O_5 + CaCO_3 \rightarrow 2CaO{\cdot}P_2O_5 + CO_2$ reaction occured and the crystalline phase formed promoted bulk crystallization of the glass. This made the system more rigid and stopped foaming.

    An analogy can be made with CPA glasses sintering behaviour, where no foaming agent was used, but in which some air was trapped. This could explain the glass shrinkage curves (Fig. 9): the crystallization stops the shrinkage, and the swelling that then occurs can be due to the trapped air expansion. That leads to large pores in CPA (without alumina, no glass micrograph in this paper) where the crystallization occurs at higher temperature than in the presence of alumina (CPA5); alumina promotes this crystal formation at the beginning of the glass shrinkage, so open porosity remains, no air is trapped, and so no swelling occurs. The CPA2 glass has an intermediate behaviour.

    The consequence of the glass behaviour, without alumina, during heating in enstatite can contribute to the formation of large pores in 15M015 that cannot be removed by the soaking at the sintering temperature.
  - Glass repartition.
    If the initial mixture is not homogeneous, the glass migrates from the zones where it was aggregated to more homogeneous regions.[13] So large pores remain in the place of glass aggregates.
  - Pore coarsening and coalescence.[13]
    Small size pores coalesced with the large ones. In the present case small pores could result of phenomena occurring during the glass crystallization. Large pores could come from heterogeneities in initial mixtures.

3.2.2 Biosteatite properties

Mechanical properties of these ceramics are shown in Table 3. Globally, lower mechanical properties were observed compared to those of single phase enstatite. Flexural strengths decreased significantly when the glass content increased, due to the porosity mentioned before (Fig. 8). Toughnesses were also lower in the presence of glass, but did not decrease with the glass content, probably due to a balance effect caused by a partial crystallization of this glass. Concerning Young's modulus it seemed that glass had the same effect whatever its composition and amount were.

An addition of 5% CPA2 glass lowered the sintering temperature by 100°C and leads to small pores, homogeneous microstructure. So this composition (15M25) had the same flexural strength and hardness compared to that of enstatite, and was chosen for machining tests.

Table 3. Sintering conditions and properties of biosteatites

Sample reference	*Wt% glass*	*Sintering temperature (°C)*	*Volumic mass (g cm^{-3})*	σ_f *±20MPa*	K_{IC} *0·1MPa.√m*	*HV ±(50)*	E *(GPa)*
15M1	0	1350	2.88	200	2·2	520	180
15M05	5-CPA	1250	2·82	200	1·6	500	130
15M010	10-CPA	1225	2·75	170	1·7	510	130
15M015	15CPA	1200	2·68	140	1·7	490	120
15M25	5-CPA2	1250	2.82	200	1·7	520	130
15M210	10-CPA2	1225	2·76	180	1·8	510	120
15M215	15CPA2	1200	2·70	170	2	470	110
15M55	5-CPA5	1250	2·82	210	1·8	560	130
15M510	10-CPA5	1225	2·76	170	1·8	520	120
15M515	15CPA5	1200	2.71	170	2.1	500	120

CPA glass: 80 wt% $CaO{\cdot}P_2O_5$ + 20 wt% $AlPO_4$·CPA2: (CPA + 2.5% Al_2O_3) glass. CPA5: (CPA + 5% Al_2O_3) glass.

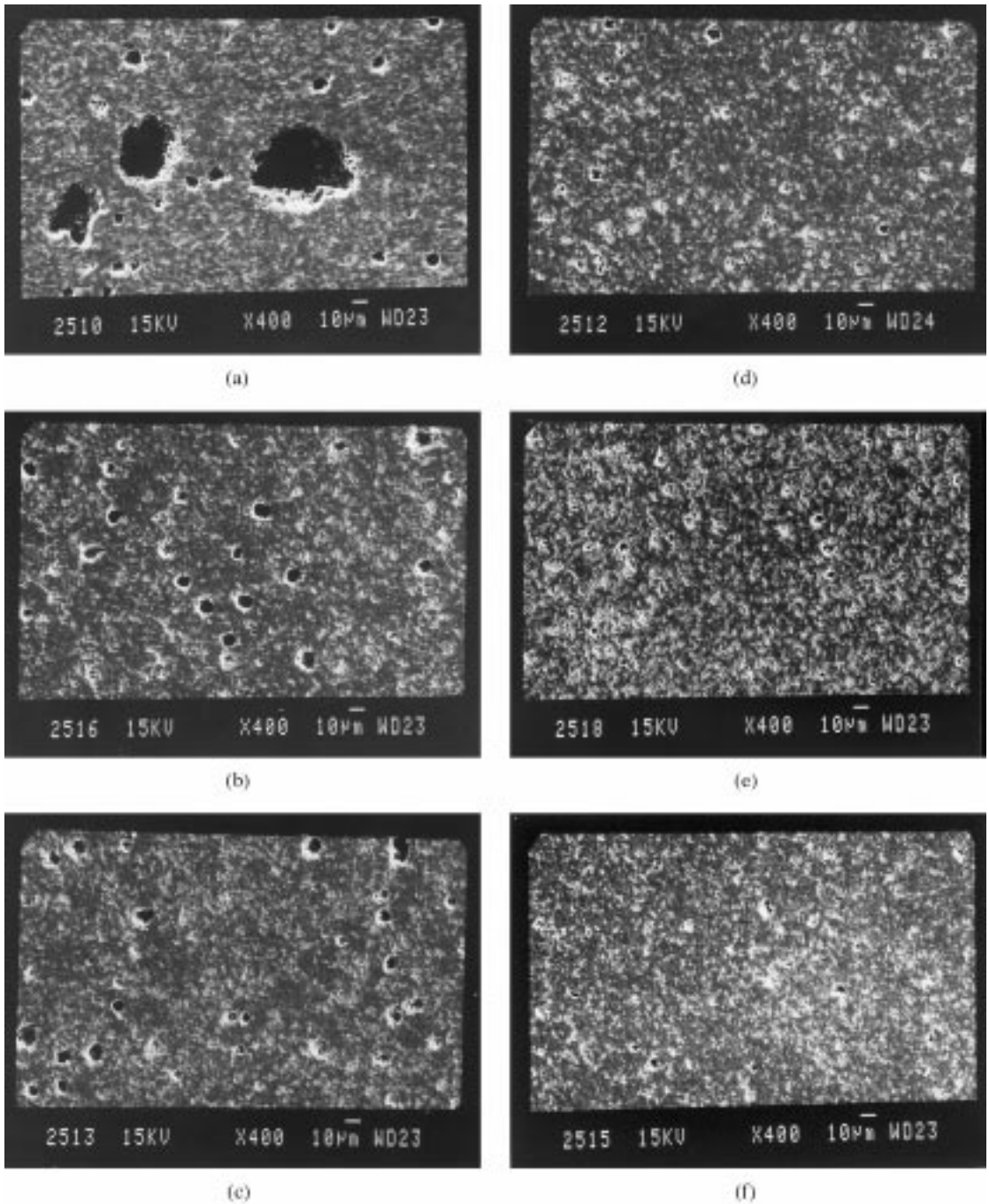

Fig. 8. Polished surfaces of different 'biosteatites': (a) 15M015: 15M1 + 15% {80wt% $CaO.P_2O_5$ + 20wt% $AlPO_4$ }(CPA) glass; (b) 15M215: 15M1 + 15% CPA + 2·5% Al_2O_3 glass; (c) 15M515: 15M1 + 15% CPA + 5% Al_2O_3 glass; (d) 15M05: 15M1 + 5% CPA glass; (e) 15M25: 15M1 + 5% CPA + 2·5% Al_2O_3 glass; (f) 15M55: 15M1 + 5% CPA + 5% Al_2O_3 glass;

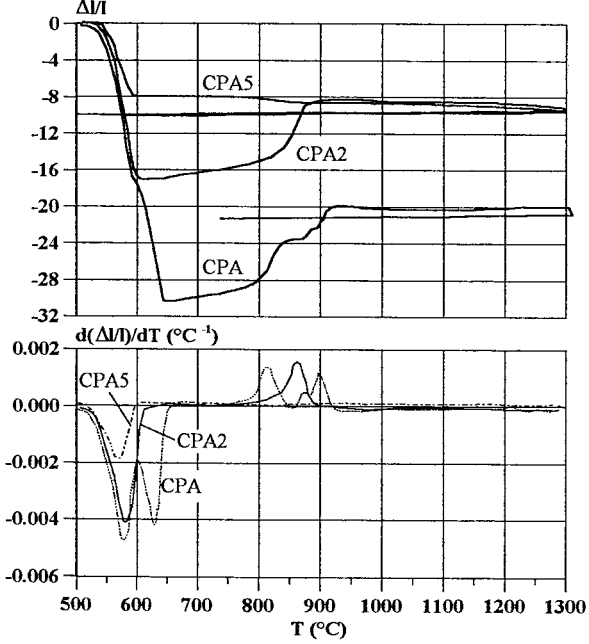

Fig. 9. Dilatometric curves for CPA (80 wt% $CaO.P_2O_5$ + 20wt% $AlPO_4$), CPA2 (CPA + 2·5% Al_2O_3) and CPA5 (CPA + 5% Al_2O_3) glasses.

3.3 Materials machinability

In a first step, we compared enstatites with elongated grains, with various grain size (15M0, 15 M1, 15 M4) and equiaxed SSC1 enstatite machinability. Those enstatite ceramics were compared with two commercial glass ceramics containing leucite: $K_2O{\cdot}Al_2O_3{\cdot}4SiO_2$ (IVOCLAR) or tetrafluoromica crystals $KMg_{2\cdot5}\ Si_4\ O_{10}\ F_2$ (DICOR from CORNING-GLASS). Machining conditions were: rotating speed $\varpi_o = 36\,000$ r.p.m., cutting depth $e = 0{\cdot}5$ mm, the load F varying from 100 to 250 g (Fig. 1).

The cutting speed was determined for each load F and the compression side of the groove was observed (Fig. 10). On the traction side many chips remained after the machining test.

Two families of materials can be considered: those with a low toughness (glass ceramics): $K_{1c} < 1$ MPa.$\sqrt{m}$, those with a higher toughness $K_{1c} > 2$ MPa.$\sqrt{m}$:

- For the first, the cutting speeds were the highest, but grooves contained a lot of chips: in this case, the abrasion occurs by chipping because of the samples brittleness. For the highest loads (upper than 200 g) the leucite based material (IVOCLAR) with the highest hardness leads to the lowest cutting speed.
- The enstatite based materials, the other family, gave higher toughnesses (and hardnesses lower or equal to those of glass ceramics); the cutting speeds were also lower but the groove did not contain macroscopic defects. In this family, the harder the material, the lower the machining speed, in relation also with a porosity decrease.

Comparing the influence of enstatite morphology on machinability is not easy, because 15M1 and SSC1 did not present exactly equivalent microstructures (grain size and porosity). It seems that the groove quality is almost the same, with a higher speed for the equiaxed morphology (SSC1).

In a second step (Fig. 11), experiments were performed on enstatites containing glassy phase (15M25), and alumina (ALCOA A16SG). The conditions were $\varpi_o = 36\,000$ r.p.m., $e = 0{\cdot}3$ mm, the

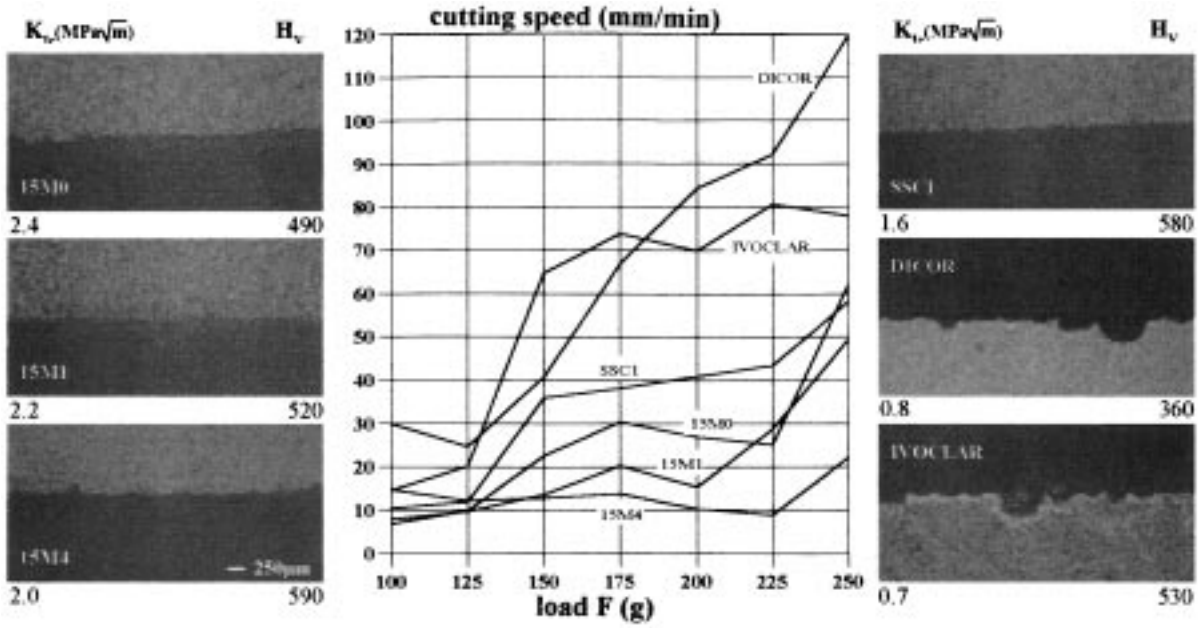

Fig. 10. Cutting speeds versus load and groove sides under compressive stress for different enstatites and commercial glass ceramics.

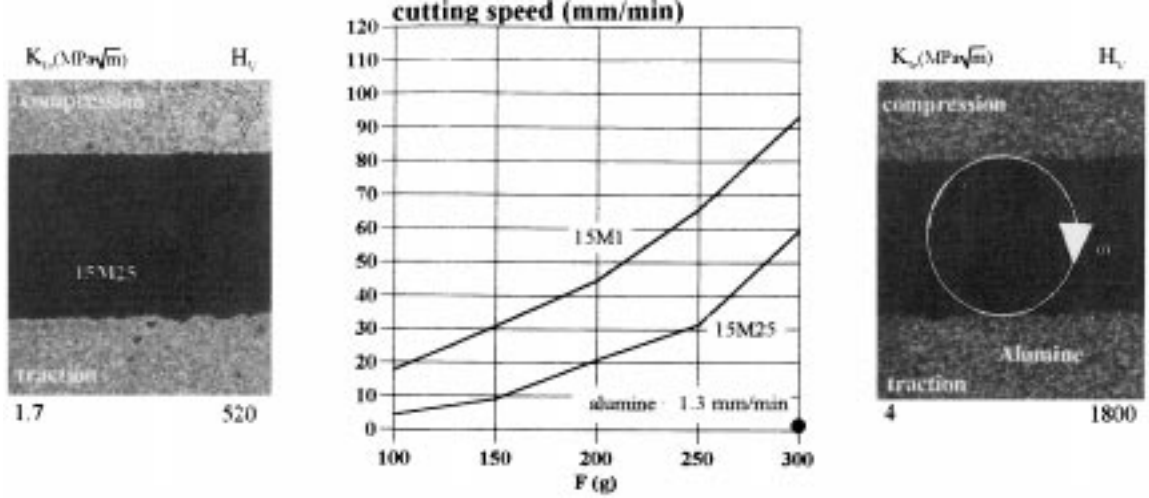

Fig. 11. Cutting speeds versus load and groove sides under compressive stress for enstatites without (15M1) and with glass (15M25), compared with alumina.

load F varying from 100 to 300 g. Glass adddition (15M25) was not favourable to the machinability. This could be explained by some porosity decrease and the glass crystallization at grain boundaries that leads to a higher material cohesion. Concerning alumina, the cutting speeds were too low to choose this material for such machining application.

3.4 Biological properties

Transmission electron microscopic (TEM) descriptions of ultra-thin sections showed the relationship between osteoblasts and 15M1 ceramics (Fig. 12). After 21 days of culture, the osteoblasts form a pluristratified cellular layering, with abundant extracellular matrix, over the whole surface of the samples. The basal cells were spread out and flat,

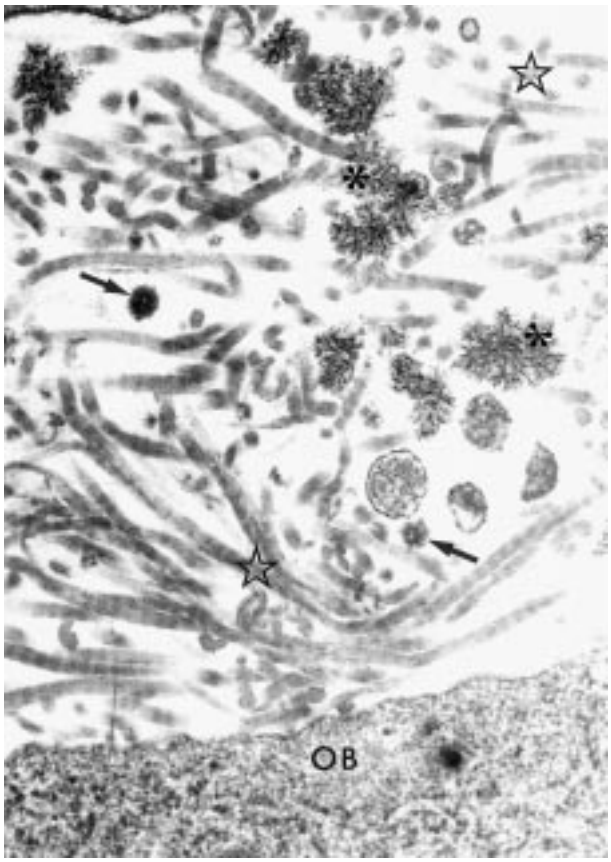

Fig. 12. Transmission electron micrograph showing mineralized bone extracellular matrix. Matrix vesicles (arrows) and clusters of needle-shaped apatite crystals (asterisks) were visible in the collagenous network (stars). Osteoblast (OB). Field width, 4 μm.

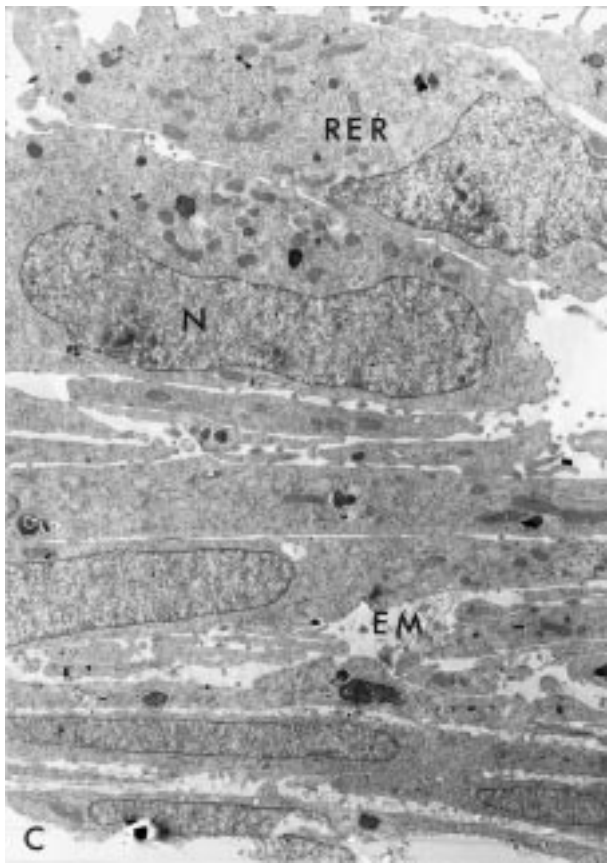

Fig. 13. Vertical cross-section of a multilayered osteoblast cultures. Adjacent to the space previously occupied by ceramic (C), the cells were flattened whereas at the top of the field they were large. Nucleus (N), Rough Endoplasmic Reticulum (RER), Extracellular Matrix (EM). Field width, 13 μm.

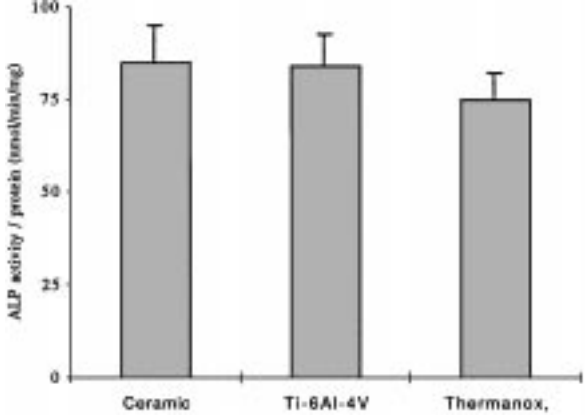

Fig. 14. Osteoblast alkaline phosphatase activity after 10 days culture on ceramic, Ti_6Al_4V and Thermanox® (mean ± s.e.m.; $n = 6$).

making close contact with the ceramic grains. In places, the osteoblasts are arranged in mineralized nodules, the formation of which is basically considered to be the final step in the differentiation and adoption of specific functions of the osteoblasts. Osteoblasts seemed to be very active, round in shape, with a large nucleus, a well-developed rough endoplasmic reticulum and numerous mitochondria. They synthesize type I collagen, and release matrix vesicles, the biochemical machinery of which includes alkaline phosphatase and leads to the formation of hydroxyapatite crystals (Fig. 13). These morphological observations are similar to those made *in vitro* and *in vivo* concerning commercially pure titanium and titanium alloy (Ti_6Al_4V), which have long been known for their osteointegrative properties.[14,15]

The alkaline phosphatase enzyme is prominently associated with osteoblast maturation and calcification and was used here as a marker. In this research, the measurement of ALP activity was used to investigate if mineralization was influenced by the surface properties of ceramic disks compared to Ti_6Al_4V and to a conventional tissue culture support: Thermanox® (modified polyethyleneterephtalate). The results were expressed as nanomoles of *p*-nitrophenol released per minute per microgram protein. As shown in Fig. 14, the alkaline phosphatase activity is higher on the ceramics than on the Thermanox®, and, more importantly, is identical to the activity measured on Ti_6Al_4V.

These findings suggest that 15M1 ceramics enhance the deposit of mineralized bone tissue and could consequently be used as implant material in maxillofacial or orthopaedic surgery. *In vitro* and *in vivo* research should, however, be pursued to determine more precisely the influence of this new machinable ceramic on the different biological phenomena contributing to bone formation (cell adhesion, cell proliferation, bone matrix synthesis, mineralization).

4 Conclusions

The present study shows it is possible to sinter talc powders after dehydration and milling without glass addition, to obtain protoenstatite based materials. The highest densities are obtained if the soaking temperature is chosen in order to avoid the proto to clinoenstatite transformation during cooling, because this transformaton leads to a volume decrease. A $CaO–P_2O_5\sqrt{}AlPO_4\sqrt{}Al_2O_3$ glass addition can be made and permits to lower slightly the sintering temperature. In comparison with some glass ceramics used in dentistry, the enstatite mechanical properties present higher toughness (up to $2{\cdot}4\,MPa{\cdot}\sqrt{m}$, instead of $0{\cdot}8\,MPa{\cdot}\sqrt{m}$) for the same flexural strength. The principal result of machinability tests is that the grooves present less chips for the enstatite materials. These materials could be good candidates for biorestorations (crowns, bones).

Acknowledgements

This work is a part of the Ph.D. thesis of Daniel Merle (Saint-Etienne, 04-12-95, n°. 134 TD)

References

1. Rekow, D., Computer-aided design and manufacturing in dentistry: a review of the state of the art. *J. Prost. Dent.*, 1987, **58**, 512–520.
2. Duret, F., La CFAO dentaire—six ans après la première présentation au congrès de l'ADF de 1985. *Actualités Odonto-stomatologiques*, 1991, **175**, 431–454.
3. Kvam, K., Fracture toughness of dental materials. *Biomaterials*, 1992, **3**(2), 101–104.
4. Exbrayat, P., Couble, M. L., Magloire, H. and Hartmann, D. J., Evaluation of the biocompatibility of a Ni–Cr–Mo dental alloy with human gingival explant culture *in vitro*: morphological study: immunodetection of fibronectine, and collagen production. *Biomaterials*, 1987, **8**, 385–392.
5. Veron, M. H., Couble, M. L. and Magloire, H., Selective inhibition of collagen synthesis by fluoride in human pulp fibroblasts *in vitro*. *Calcif. Tissue Int.*, 1993, **53**, 38–44.
6. Forster, W. R., High temperature X-ray diffraction study of the polymorphism of $MgSiO_3$. *J. Am. Ceram. Soc.*, 1951, **34**(9), 255–259.
7. Lee, W. E. and Heuer, A. H., On the polymorphism of enstatite. *J. Am .Ceram. Soc.*, 1987, **70**(5), 349–360.
8. Brown, W. L., Morimoto, N. and Smith, J. V., A structural explanation of the polymorphism and transitions of $MgSiO_3$. *J. Geol.*, 1961, **69**, 609–616.
9. Huang, C. M., Kuo, D. H., Kim, Y. J. and Kriven, W. M., Phase stability of chemically derived enstatite ($MgSiO_3$). *J. Am. Ceram. Soc.*, 1994, **77**(10), 2625–2631.
10. Sarver, J. F. and Hummel, F. A., Stability relations of magnesium metasilicate polymorphs. *J. Am. Ceram. Soc.*, 1962, **45**(4), 152–156.
11. Harmer, M. P., Chan, H. M. and Miller, G. A., Unique opportunities for microstructural engineering with duplex

and laminar ceramic composites. *J. Am. Ceram. Soc.*, 1992, **75**(7), 1715–1728.
12. Pernot, F., Zarzycki, J., Bonnel, F., Rabichong, P. and Baldet, P., New glass-ceramic materials for prosthetic applications. *J. Am. Ceram. Soc.*, 1979, **14**(7), 1694–1706.
13. Bernache-Assolant, D., Chimie-physique du Frittage, Editions Hermès, Paris, 1993.
14. Bouvier, B., Martin, J. M., Exbrayat, P., Rigollet, E., Le Mogne, T., Treheux, D. and Magloire, H., Ultrastructural study of calvaria-released osteoblasts cultured in contact with titanium-based substrates. *Cells and Materials*, 1994, **4**, 135–142.
15. Nanci, A., McCarthy, G. F., Zalzal, S., Clokie, C. M. L., Warshawsky, H. and McKee, M. D., Tissue response to titanium implants in the rat tibia: ultrastructural, immunocytochemical and lectin-cytochemical characterization of the bone–titanium interface. *Cells and Materials*, 1994, **4**, 1–30.